
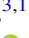






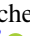
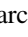







# No Evidence for Enhanced [O III] 88 $\mu\text{m}$ Emission in a $z \sim 6$ Quasar Compared to Its Companion Starbursting Galaxy

Fabian Walter<sup>1,2</sup> , Dominik Riechers<sup>3,1</sup> , Mladen Novak<sup>1</sup>, Roberto Decarli<sup>4</sup> , Carl Ferkinhoff<sup>5</sup> , Bram Venemans<sup>1</sup> , Eduardo Bañados<sup>6</sup>, Frank Bertoldi<sup>7</sup> , Chris Carilli<sup>2</sup>, Xiaohui Fan<sup>8</sup> , Emanuele Farina<sup>9</sup> , Chiara Mazzucchelli<sup>10</sup> , Marcel Neeleman<sup>1</sup> , Hans-Walter Rix<sup>1</sup>, Michael A. Strauss<sup>11</sup> , Bade Uzgil<sup>2,1</sup> , and Ran Wang<sup>12</sup> 

<sup>1</sup>Max Planck Institute for Astronomy, Königstuhl 17, D-69117 Heidelberg, Germany; [walter@mpia.de](mailto:walter@mpia.de)

<sup>2</sup>National Radio Astronomy Observatory, Pete V. Domenici Array Science Center, P.O. Box O, Socorro, NM 87801, USA

<sup>3</sup>Cornell University, 220 Space Sciences Building, Ithaca, NY 14853, USA

<sup>4</sup>INAF Osservatorio di Astrofisica e Scienza dello Spazio, via Gobetti 93/3, I-40129, Bologna, Italy

<sup>5</sup>Winona State University, Winona, MN 55987, USA

<sup>6</sup>The Observatories of the Carnegie Institution for Science, 813 Santa Barbara Street, Pasadena, CA 91101, USA

<sup>7</sup>Argelander-Institut für Astronomie, Universität Bonn, Auf dem Hügel 71, D-53121 Bonn, Germany

<sup>8</sup>Steward Observatory, The University of Arizona, 933 North Cherry Avenue, Tucson, AZ 85721, USA

<sup>9</sup>University of California Santa Barbara, Santa Barbara, CA, USA

<sup>10</sup>European Southern Observatory, Alonso de Córdova 3107, Vitacura, Región Metropolitana, Chile

<sup>11</sup>Department of Astrophysical Sciences, Princeton University, Princeton, NJ 08544, USA

<sup>12</sup>Kavli Institute of Astronomy and Astrophysics at Peking University, No.5 Yiheyuan Road, Haidian District, Beijing, 100871, People's Republic of China

Received 2018 November 15; revised 2018 November 29; accepted 2018 November 30; published 2018 December 13

## Abstract

We present Atacama Large Millimeter/submillimeter Array band 8 observations of the [O III] 88  $\mu\text{m}$  line and the underlying thermal infrared continuum emission in the  $z = 6.08$  quasar CFHQS J2100–1715 and its dust-obscured starburst companion galaxy (projected distance:  $\sim 60$  kpc). Each galaxy hosts dust-obscured star formation at rates  $> 100 M_{\odot} \text{yr}^{-1}$ , but only the quasar shows evidence for an accreting  $10^9 M_{\odot}$  black hole. Therefore we can compare the properties of the interstellar medium in distinct galactic environments in two physically associated objects,  $\sim 1$  Gyr after the big bang. Bright [O III] 88  $\mu\text{m}$  emission from ionized gas is detected in both systems; the positions and linewidths are consistent with earlier [C II] measurements, indicating that both lines trace the same gravitational potential on galactic scales. The [O III] 88  $\mu\text{m}$ /far-infrared (FIR) luminosity ratios in both sources fall in the upper range observed in local luminous infrared galaxies of similar dust temperature, although the ratio of the quasar is smaller than in the companion. This suggests that gas ionization by the quasar (expected to lead to strong optical [O III] 5008 Å emission) does not dominantly determine the quasar's FIR [O III] 88  $\mu\text{m}$  luminosity. Both the inferred number of photons needed for the creation of  $\text{O}^{++}$  and the typical line ratios can be accounted for without invoking extreme (top-heavy) stellar initial mass functions in the starbursts of both sources.

**Key words:** galaxies: high-redshift – galaxies: ISM – quasars: emission lines – quasars: general – submillimeter: ISM

## 1. Introduction

The most distant quasars at  $z > 6$  are unique probes of galaxy and structure formation in the first Gigayear of the universe. Their rapidly accreting supermassive black holes make these quasars the most luminous (non-transient) sources known at this cosmic epoch (e.g., Fan et al. 2006; Venemans et al. 2015; Wu et al. 2015; Bañados et al. 2016). The interstellar medium (ISM) of more than 30 host galaxies of  $z \sim 6$  quasars has now been detected through the [C II] 158  $\mu\text{m}$  line (hereafter: [C II]) and far-infrared (FIR) continuum emission. This suggests that the host galaxies have intense star formation rates (SFRs) at many hundreds of  $M_{\odot} \text{yr}^{-1}$  occurring coevally with the growth of the accreting central black holes (e.g., Bertoldi et al. 2003; Walter et al. 2003, 2009; Wang et al. 2013; Willott et al. 2013, 2015; Decarli et al. 2018; Venemans et al. 2018).

Using Atacama Large Millimeter/submillimeter Array (ALMA) observations, Decarli et al. (2017) found dust-obscured companions to four quasars in a [C II] survey of 27  $z \sim 6$  quasars. These massive star-forming companion galaxies show no signs of powerful active galactic nucleus (AGN) activity and were detected serendipitously within 8–60 kpc at the same redshifts in four systems, suggesting that they are

physically associated with overdensities or proto-clusters of galaxies at  $z > 6$ . These companion galaxies rival the FIR and [C II] luminosities of the neighboring quasars, in some cases even surpassing their (already extreme) luminosity. These quasar–galaxy pairs thus provide a unique opportunity to efficiently study the ISM in distinctly different galactic environments in the first Gyr of the universe: pure starbursts, and those in the presence of a powerful AGN.

To date, the [C II] line has been the workhorse line of ISM studies at  $z > 6$  (e.g., Carilli & Walter 2013), but it is only one of several fine structure lines that help to characterize the physical properties of the ISM (e.g., Díaz-Santos et al. 2017). Of these, the [O III] 88  $\mu\text{m}$  line ( ${}^3\text{P}_1 \rightarrow {}^3\text{P}_0$ ) (hereafter: [O III]<sub>88</sub>), emitted by doubly ionized oxygen ( $\text{O}^{++}$ ), is a particularly important diagnostic of the star formation process (e.g., Ferkinhoff et al. 2010, 2011, 2015; Vishwas et al. 2018): Given the  $\text{O}^+$  ionization potential of 35.1 eV,  $\text{O}^{++}$  is almost exclusively found in dense H II regions around O-type stars or in AGN environments. Indeed, an enhancement of the optical 5008 Å [O III] line is a key diagnostic of AGN activity (e.g., Baldwin et al. 1981). In contrast, neutral carbon has an ionization potential of only 11.3 eV, and [C II] is therefore emitted both in the neutral and ionized phase. So far, [O III]<sub>88</sub>

detections have been reported in a number of  $z > 6$  galaxies (e.g., Inoue et al. 2016; Carniani et al. 2017; Laporte et al. 2017; Hashimoto et al. 2018b, 2018a; Marrone et al. 2018; Tamura et al. 2018). However, in this redshift range, only two systems have been detected in [O III]<sub>88</sub>, [C II], and the underlying dust continuum: the Lyman break galaxy B14–65666 at  $z = 7.15$  (Hashimoto et al. 2018a) and the lensed galaxy SPT0311–58 at  $z = 6.90$  (Marrone et al. 2018, the latter actually consists of two sources).

In this Letter we report [O III]<sub>88</sub> and underlying dust continuum observations with ALMA of the  $z = 6.08$  quasar CFHQS J2100–1715 (hereafter J2100–Q) and its dust-enshrouded companion starburst (J2100–SB). J2100–Q was discovered by Willott et al. (2010b), and a black hole mass of  $(9.4 \pm 2.6) \times 10^8 M_\odot$  was reported in Willott et al. (2010a). J2100–SB was discovered by Decarli et al. (2017) in the FIR using ALMA. Multi-wavelength follow-up observations of the companion galaxy using *Spitzer* (3.6  $\mu\text{m}$ , 4.5  $\mu\text{m}$ ) and *Hubble Space Telescope* (WFC3/140W) as well as Multi Unit Spectroscopic Explorer (MUSE) and Large Binocular Telescope (LBT) spectroscopy did not detect the companion in the rest-frame ultraviolet (UV)/optical, with an implied ratio of obscured to un-obscured star formation of  $>99\%$  (C. Mazzucchelli et al. 2018, in preparation). No metallicity measurement of our targets exists, but they must be significantly enriched with heavy elements as they harbor significant amounts of dust, and have high ( $\sim 100 M_\odot \text{yr}^{-1}$ ) SFRs.

In Section 2 we describe our ALMA band 8 observations, in Section 3 we present our results, followed by a discussion and a summary in Sections 4 and 5. Throughout this Letter we use cosmological parameters  $H_0 = 70 \text{ km s}^{-1} \text{ Mpc}^{-1}$ ,  $\Omega_M = 0.3$ , and  $\Omega_\Lambda = 0.7$ , leading to a scale of 5.67 kpc per arcsec at the redshift of our sources.

## 2. Observations

We observed the [O III]<sub>88</sub> line ( $\nu_{\text{rest}} = 3393.0062 \text{ GHz}$ ) of J2100–Q and J2100–SB redshifted to  $\nu_{\text{obs}} = 479.2 \text{ GHz}$  at  $z = 6.08$  with ALMA in band 8 and configuration C43–1 on 2018 May 20 (two executions) and 2018 May 23 (one execution) for a total of  $3 \times 5200 \text{ s}$  or 4.3 hr, of which 2.5 hr were spent on source. The redshifts of the sources were known from the earlier detections of [C II] line emission ( $z = 6.0806 \pm 0.0011$  for the quasar,  $6.0796 \pm 0.0008$  for the companion). The two sources are very close in redshift ( $\Delta v_{\text{LOS}} = 41 \text{ km s}^{-1}$ , Decarli et al. 2017), meaning that the [O III]<sub>88</sub> emission in the two objects could be covered with the same frequency setup. However, the projected separation on the sky ( $\sim 11''$ ) required two pointings to cover the sources in band 8. The software package CASA (McMullin et al. 2007) was used for data reduction and imaging. For optimal sensitivity, we employed natural weighting when imaging the data, leading to a synthesized beam size of  $0''.73 \times 0''.56$  ( $\sim 3.7 \text{ kpc}$  at  $z = 6.08$ ), and an rms of  $0.45 \text{ mJy beam}^{-1}$  per  $50 \text{ km s}^{-1}$  (80 MHz) channel. The corresponding sensitivity in the continuum (excluding the channels that contain line emission) is  $54 \mu\text{Jy beam}^{-1}$  over an effective bandwidth of 5.625 GHz. For all analysis of the [O III]<sub>88</sub> line data, the continuum has been subtracted in the  $uv$ -plane using line-free channels.

We also re-analyzed the [C II] and underlying continuum ALMA data published by Decarli et al. (2017) and Venemans et al. (2018). The beam size of these [C II] data ( $0''.73 \times 0''.57$ ) is almost identical to that presented here. Therefore, no

**Table 1**  
[O III]<sub>88</sub> and Rest-frame 88  $\mu\text{m}$  Continuum Measurements of the Quasar CFHQS J2100–Q and Its Companion J2100–SB

	Units	Quasar	Companion
$z_{[\text{O III}]88}$		$6.0816 \pm 0.0009$	$6.0806 \pm 0.0005$
$S_{\text{cont},88 \mu\text{m}}^{\text{a}}$	$\text{mJy beam}^{-1}$	$1.12 \pm 0.05$	$2.87 \pm 0.05$
$S_{\text{cont},158 \mu\text{m}}^{\text{a,b}}$	$\text{mJy beam}^{-1}$	$0.46 \pm 0.07$	$1.37 \pm 0.14$
$S_{[\text{O III}]88}^{\text{c}}$	$\text{mJy beam}^{-1}$	$0.93 \pm 0.20$	$2.55 \pm 0.21$
$\text{FWHM}_{[\text{O III}]88}^{\text{c}}$	$\text{km s}^{-1}$	$454 \pm 117$	$614 \pm 62$
$F_{[\text{O III}]88}^{\text{d}}$	$\text{Jy km s}^{-1}$	$0.39 \pm 0.06$	$1.52 \pm 0.07$
$F_{[\text{C II}]}^{\text{d}}$	$\text{Jy km s}^{-1}$	$1.09 \pm 0.08$	$1.89 \pm 0.21$
$T_{\text{dust}}$	K	$41 \pm 1.2$	$37 \pm 1.2$
$L_{\text{IR}[8-1000 \mu\text{m}]}$	$10^{11} L_\odot$	$8.3 \pm 0.37$	$19.1 \pm 0.33$
$L_{\text{FIR}[42-122 \mu\text{m}]}$	$10^{11} L_\odot$	$6.8 \pm 0.30$	$15.5 \pm 0.28$
$L_{[\text{O III}]88}$	$10^9 L_\odot$	$0.77 \pm 0.12$	$2.86 \pm 0.13$
$L_{[\text{C II}]}$	$10^9 L_\odot$	$1.05 \pm 0.08$	$1.81 \pm 0.9$
$L_{[\text{O III}]88}/L_{[\text{C II}]}$		$0.74 \pm 0.15$	$1.58 \pm 0.24$
$L_{[\text{O III}]88}/L_{\text{FIR}}$	$10^{-3}$	$1.12 \pm 0.11$	$1.86 \pm 0.14$
$L_{[\text{C II}]} / L_{\text{FIR}}$	$10^{-3}$	$1.55 \pm 0.13$	$1.17 \pm 0.13$

**Notes.** Re-measured [C II] and rest-frame 158  $\mu\text{m}$  continuum values from Decarli et al. (2017). All measurements obtained at continuum emission peak.

<sup>a</sup> Observed continuum flux density underlying the line emission.

<sup>b</sup> The error of the companion is higher as it is not in the phase center.

<sup>c</sup> From Gaussian fitting to the line.

<sup>d</sup> Based on integrated line maps (values consistent with spectra).

additional beam matching was required. In order to optimize the signal-to-noise ratio in the measurements, and given the fact that any extent, if present, is marginal, we extract [C II] line and underlying continuum fluxes at the peak position of both sources. We report the [C II] values adopted in this study in Table 1.<sup>13</sup>

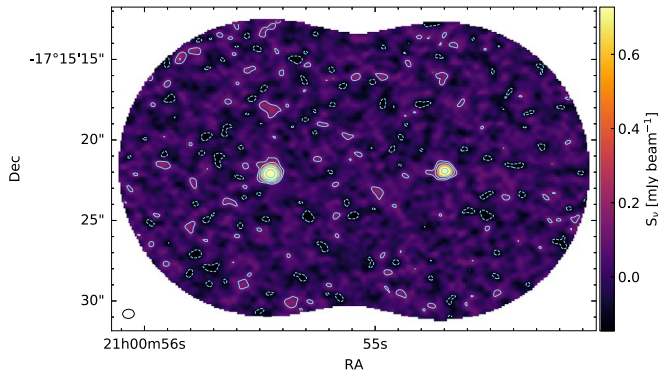
## 3. Results

### 3.1. Continuum Emission

In Figure 1 we show the rest-frame 88  $\mu\text{m}$  (observed: 475 GHz) continuum map of J2100–Q and J2100–SB. This map is based on those channels in the datacube that do not contain the [O III]<sub>88</sub> line. The sources are detected at high significance and are unresolved at the resolution of our beam ( $0''.73 \times 0''.57$ , flux densities are reported in Table 1). The coordinates (R.A./decl. in J2000.0) of the sources, 21:00:54.70,  $-17:15:21.9$  (J2100–Q), and 21:00:55.45,  $-17:15:21.7$  (J2100–SB) are in agreement with Decarli et al. (2017).

Together with our earlier rest-frame 158  $\mu\text{m}$  continuum measurement around the [C II] line (Decarli et al. 2017, see Table 1 for slightly updated numbers) we can use the new rest-frame 88  $\mu\text{m}$  observations to further constrain the properties of the FIR continuum emission. The infrared (IR) and FIR luminosities are obtained by fitting the 88 and 158  $\mu\text{m}$  data

<sup>13</sup> We note that both Decarli et al. (2017) and Venemans et al. (2018) report [C II] and FIR luminosities that are slightly higher than the values adopted here, as their reported fluxes are based on 2D fitting of the line emission in the image domain.



**Figure 1.** Rest-frame  $88\ \mu\text{m}$  continuum emission of the  $z = 6.08$  quasar J2100-Q (Western source) and its companion J2100-SB (Eastern source). Logarithmically spaced contours are shown at  $\pm 2, 4, 8, \dots \sigma$ , with  $\sigma = 54\ \mu\text{Jy beam}^{-1}$ . The beam size of  $0''.73 \times 0''.57$  (position angle:  $87^\circ 3$ ) is shown in the bottom-left corner. Two pointings were needed to cover both sources in ALMA band 8.

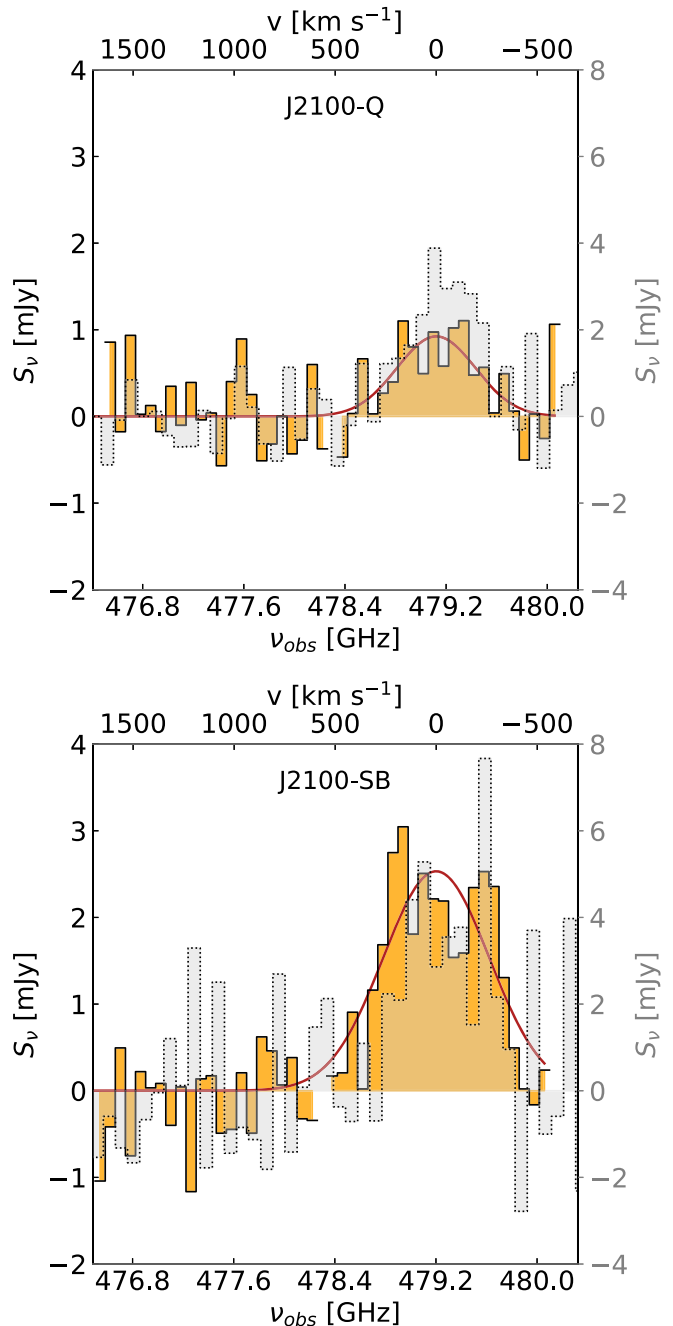
points (assuming that they are optically thin) with a modified blackbody, taking the effect of the cosmic microwave background into account (da Cunha et al. 2013). These results are reported in Table 1. The resulting  $L_{\text{IR}}$ -based SFRs (Kennicutt & Evans 2012) are  $125 \pm 14 M_\odot \text{yr}^{-1}$  (J2100-Q) and  $284 \pm 30 M_\odot \text{yr}^{-1}$  (J2100-SB).

### 3.2. $[\text{O III}]_{88}$ Line Emission

We show the continuum-subtracted  $[\text{O III}]_{88}$  spectra of both sources in Figure 2 as extracted from the peak positions of the continuum map. The Gaussian fit results are reported in Table 1. For reference, we overplot scaled, continuum-subtracted  $[\text{C II}]$  spectra from Decarli et al. (2017) in grayscale. Both the redshifts and the linewidths of the  $[\text{O III}]_{88}$  and  $[\text{C II}]$  detections agree within the uncertainties. The  $[\text{O III}]_{88}$  line width of the quasar is much smaller than that of emission lines seen in the broadline region of the quasar (FWHM:  $\sim 3600\ \text{km s}^{-1}$ , Willott et al. 2010a). In Figure 3 we show the integrated  $[\text{O III}]_{88}$  maps of both sources, after continuum subtraction. 2D-Gaussian fitting shows that the  $[\text{O III}]_{88}$  line emission is unresolved at our resolution like the continuum emission. In Table 1 we summarize the resulting  $[\text{O III}]_{88}$  luminosities. Using the  $[\text{O III}]_{88}$ -SFR scaling relations of De Looze et al. (2014) for their “high-redshift sample” we derive  $[\text{O III}]_{88}$ -based SFRs of approximately  $100 M_\odot \text{yr}^{-1}$  and  $360 M_\odot \text{yr}^{-1}$  for the quasar and the companion, respectively, consistent with the FIR-based estimates (Section 3.1).

### 3.3. Line/FIR Luminosity Ratio

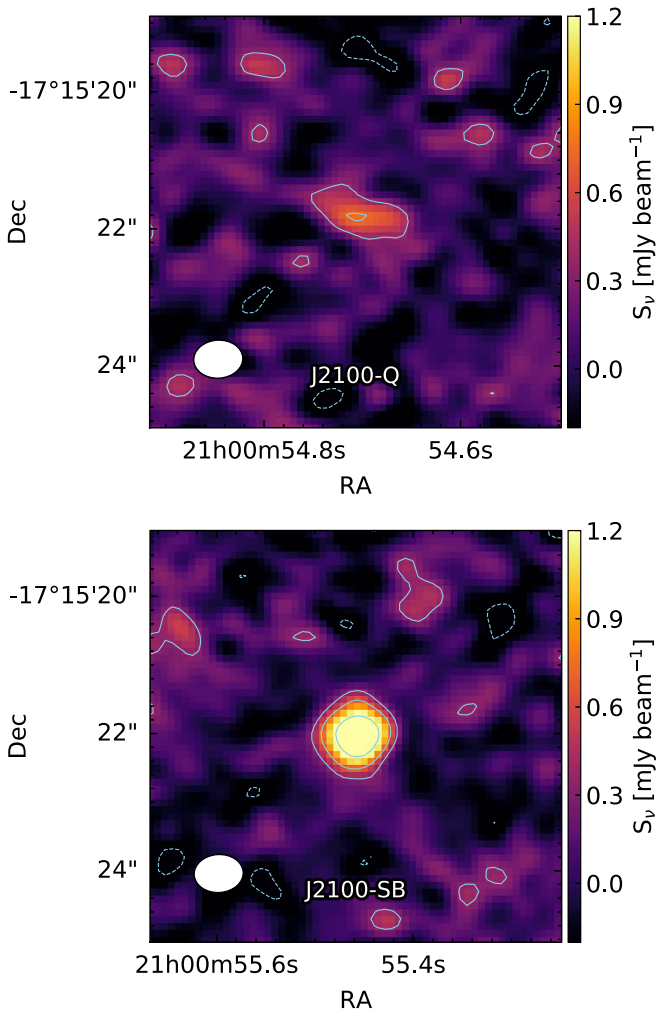
We now combine the  $[\text{O III}]_{88}$  and rest-frame  $88\ \mu\text{m}$  continuum measurements with the earlier  $[\text{C II}]$  line measurements to constrain the properties of the ISM in our targets. This is particularly interesting, as our sources are physically quite different. In Figure 4 (left panel) we plot the  $[\text{O III}]_{88}/\text{FIR}$  luminosity ratios versus the continuum flux density ratios ( $S_{88\ \mu\text{m}}/S_{158\ \mu\text{m}}$ ) of our sources, the latter being a proxy for the temperature of the dust (color-coded by FIR luminosity), and compare them to the recent compilation of local luminous infrared galaxies (LIRGs) by Díaz-Santos et al. (2017). The mid-infrared (MIR) emission in the majority of the local sample is not dominated by AGN emission (circles versus stars in Figure 4).



**Figure 2.**  $[\text{O III}]_{88}$  emission line spectra of J2100-Q (top panel) and J2100-SB (bottom panel) after continuum subtraction. The red line shows the Gaussian fit (parameters reported in Table 1). In grayscale, we overplot the respective spectra of the  $[\text{C II}]$  line (after shifting to the same rest-frame velocity as the  $[\text{O III}]_{88}$ ), again after continuum subtraction. The  $[\text{C II}]$  spectrum has been scaled down in intensity by a factor of 2 (axis labels to the right).

Our two sources have luminosities at the high end of the LIRG sample studied in Díaz-Santos et al. (2017), but their  $[\text{O III}]_{88}/\text{FIR}$  luminosity ratios lie only slightly above the average LIRG value of similar dust temperature, within the scatter found locally. Perhaps unexpectedly, despite the presence of an accreting  $10^9 M_\odot$  black hole, the quasar does not show enhanced  $[\text{O III}]_{88}$  emission compared to either the companion or the local comparison sample.

It is instructive to also compare the  $[\text{C II}]/\text{FIR}$  luminosity ratios for our sources to the local LIRGs (middle panel of



**Figure 3.**  $[\text{O III}]_{88}$  emission after continuum subtraction in J2100–Q (top panel) and J2100–SB (bottom panel), integrated over a velocity range of  $1.2 \times \text{FWHM}$ , respectively. Logarithmically spaced contours are shown at  $\pm 2, 4, 8\sigma$ , with  $\sigma = 0.17 \text{ mJy beam}^{-1}$  for J2100–Q and  $\sigma = 0.16 \text{ mJy beam}^{-1}$  for J2100–SB. The beam size of  $0''.73 \times 0''.57$  (position angle:  $87^\circ.3$ ) is shown in the bottom-left corner.

Figure 4). The  $[\text{C II}]/\text{FIR}$  luminosity ratios of our targets ( $\sim 1.6 \times 10^{-3}$ ) are located within the distribution observed for the local LIRGS at the same temperature (around  $\sim 1 \times 10^{-3}$ ). The right panel in Figure 4 shows the  $[\text{O III}]_{88}/[\text{C II}]$  luminosity ratios as a function of dust temperature. Again, our two targets fall within the distribution seen in local LIRGS, and the  $[\text{O III}]/[\text{C II}]$  ratio is actually *lower* in the quasar compared to the companion.

## 4. Discussion

### 4.1. Origin of the $[\text{C II}]$ and $[\text{O III}]_{88}$ Emission

The linewidths and positions of the  $[\text{O III}]$  and  $[\text{C II}]$  emission are identical within the uncertainties, which indicates that they trace the same gravitational potential on galactic scales (e.g., Carniani et al. 2017). Díaz-Santos et al. (2017) show that the ratio of the  $[\text{C II}]$  emission emerging from photodissociation regions, to that from ionized gas, is correlated with  $S_{63 \mu\text{m}}/S_{158 \mu\text{m}}$  (see their Figure 3). We determine the  $S_{63 \mu\text{m}}/S_{158 \mu\text{m}}$  ratio from our  $S_{88 \mu\text{m}}/S_{158 \mu\text{m}}$  measurements assuming the same blackbody parameters as in Section 3.1 (see

also Table 1), finding  $S_{63 \mu\text{m}}/S_{158 \mu\text{m}} = 1.7$  for the quasar, and 1.8 for the companion, respectively.

If the correlations of Díaz-Santos et al. (2017) hold, then more than 80% of the  $[\text{C II}]$  emission in both the quasar and the companion are from the neutral phase of the ISM ( $L_{[\text{C II}]^{\text{ionized}}} < 0.2 L_{[\text{C II}]}$ ). This is in contrast to the  $[\text{O III}]_{88}$  emission, which only traces the ionized phase, because the  $\text{O}^+$  ionization potential is 35.1 eV (the next ionization level is at 54.9 eV, e.g., Kramida et al. 2018). Following Ferkinhoff et al. (2010, 2011) and Vacca et al. (1996), a blackbody with a temperature  $> 35,000 \text{ K}$  ( $> 45,000 \text{ K}$ ) produces significant emission of photons with energies  $> 35 \text{ eV}$  ( $> 55 \text{ eV}$ ). These temperatures correspond to stars of type O7V and O3V, respectively.

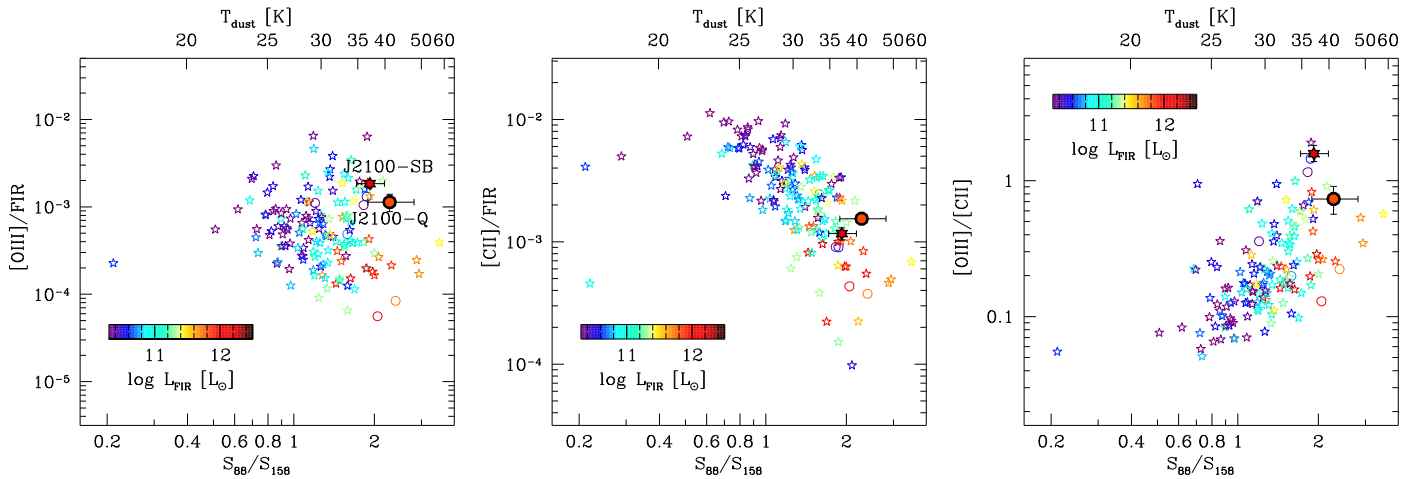
The presence of a FUV-bright central source (i.e., the accreting black hole in J2100–Q) will lead to optical  $5008 \text{ \AA}$   $[\text{O III}]$  line emission in the broadline region (e.g., Vanden Berk et al. 2001) and the narrow line region (e.g., Baldwin et al. 1981) that will become accessible to the *James Webb Space Telescope (JWST)* at  $z = 6.08$ . The FIR  $[\text{O III}]_{88}$  line on the other hand is likely to arise from stellar H II regions given that it has the same systemic velocity and line width as the  $[\text{C II}]$  line, and is much narrower than the optical lines emerging from the BLR. Additionally, the  $[\text{O III}]_{88}/\text{FIR}$  and  $[\text{O III}]_{88}/[\text{C II}]$  ratios are similar to those seen for systems where the emission is known to arise from H II regions.

### 4.2. Minimum Ionized Gas Mass

We can infer the mass of doubly ionized oxygen in our targets from the observed  $[\text{O III}]_{88}$  luminosity (see, e.g., Ferkinhoff et al. 2011) to be  $M(\text{O}^{++})/M_{\odot} = 2.55 \times 10^{-4} L_{[\text{O III}]_{88}}/L_{\odot} = 1.7 \times 10^5 M_{\odot}$  for the quasar, and  $7.3 \times 10^5 M_{\odot}$  for the companion. Assuming that most of the oxygen is in doubly ionized form, and that the oxygen abundance is  $\chi(\text{O}/\text{H}) = 5.9 \times 10^{-4}$  (Savage & Sembach 1996), this implies a minimum mass of ionized gas of  $M_{\text{min}}(\text{H}^+) = 2.1 \times 10^7 M_{\odot}$  for the J2100–Q, and  $M_{\text{min}}(\text{H}^+) = 7.7 \times 10^7 M_{\odot}$  for J2100–SB. Other high- $z$  systems have shown  $\text{O}^{++}/\text{O}$  fractions of  $\sim 10\%$  (Ferkinhoff et al. 2011), so that the actual ionized gas mass could be a factor of 10 higher than our minimum value here. Using the dust mass estimates of  $3.2 \times 10^8 M_{\odot}$  and  $5.5 \times 10^8 M_{\odot}$  derived for J2100–Q and J2100–SB, respectively (Decarli et al. 2017), and assuming a standard gas-to-dust ratio of  $\sim 100$  (Draine et al. 2007; Sandstrom et al. 2013), the molecular gas content ( $M(\text{H}_2)$ ) in both sources is  $> 10^{10} M_{\odot}$ . A ratio of  $M_{\text{min}}(\text{H}^+)/M(\text{H}_2) \sim 10^{-3}$  is similar to what is found in nearby galaxies (Brauer et al. 2008, see also the compilation in Ferkinhoff et al. 2011, their Figure 3). The total ionized gas mass is thus only a small fraction of the total mass of the dense ISM (and thus baryonic mass) in the two objects.

### 4.3. Minimum Number of Ionizing Photons and Stars

Following Ferkinhoff et al. (2010, 2011, 2015) and Vishwas et al. (2018), we calculate minimum  $\text{O}^+$ -ionizing photon rates for J2100–Q and the J2100–SB of  $Q_0 = (1.24 \pm 0.27) \times 10^{54} \text{ s}^{-1}$  and  $Q_0 = (4.62 \pm 0.20) \times 10^{54} \text{ s}^{-1}$ , respectively. It is interesting to compare this number with back-of-the-envelope expectations based on the observed SFR. The companion galaxy has an SFR  $\approx 300 M_{\odot} \text{ yr}^{-1}$ . The stars that provide significant radiation energetic enough to doubly ionize oxygen live only for  $\lesssim 5 \text{ Myr}$ . Assuming that the SFR is constant, we infer the total stellar mass created in the last 5 Myr, and



**Figure 4.** Line/FIR ratios of the  $z = 6.08$  quasar J2100–Q and its companion J2100–SB compared to the local LIRG compilation by Díaz-Santos et al. (2017). The data points are color-coded by FIR luminosity, circles (stars) mark sources with an AGN contribution of  $>50\%$  ( $<50\%$ ) in the MIR (Díaz-Santos et al. 2017). Left panel:  $[\text{O III}]_{88}/\text{FIR}$  luminosity ratio as a function of the continuum flux density ratio ( $S_{88 \mu\text{m}}/S_{158 \mu\text{m}}$ ). This ratio is a proxy for the temperature as shown on the top  $x$ -axis, assuming a modified blackbody with  $\beta = 1.6$  for the dust emissivity. Middle and right panels: same  $x$ -axis as in the left panel but now showing the  $[\text{C II}]/\text{FIR}$  luminosity ratio and the  $[\text{O III}]/[\text{C II}]$  ratio, respectively.

distribute it over different stellar mass bins based on a Chabrier (2003) initial mass function (IMF). The stellar main sequence provides us with an estimate of the luminosity and effective temperature of stars (assuming a simple blackbody) based on their mass, thus we can compute for each stellar mass bin how many photons are produced with energy  $h\nu > 35.1$  eV, needed to ionize O II. By integrating over the stellar mass distribution, scaled to match the total mass of stars produced in 5 Myr, we obtain  $Q_{0,\text{exp}} = 2.6 \times 10^{55} \text{ s}^{-1}$  (this number changes to  $Q_{0,\text{exp}} = 2.3 \times 10^{55} \text{ s}^{-1}$  for a Kroupa 2001 IMF). This number is slightly higher than the one inferred from our  $[\text{O III}]$  observations (we get similar results for J2100–Q). This suggests that star formation with a standard IMF is sufficient to account for the observed  $[\text{O III}]$  luminosity, with no need to invoke a top-heavy IMF or a contribution by a “buried” quasar.

## 5. Summary

We present ALMA  $[\text{O III}]_{88}$  observations of the  $z = 6.08$  quasar J2100–Q and its dust-enshrouded starburst companion J2100–SB. This system is unique, as it offers the possibility to study the physical properties of the ISM of two starbursts that are physically associated with each other within 1 Gyr of the big bang. They display distinct galactic environments: one source shows the presence of a powerful AGN, while the other does not. Interestingly, we find that the  $[\text{O III}]_{88}/\text{FIR}$  luminosity ratio of the starburst companion J2100–SB is higher than that of the quasar J2100–Q, even though the accreting supermassive black hole in the latter provides additional photons with energies high enough to produce  $\text{O}^{++}$  (which typically leads to strong optical 5008 Å  $[\text{O III}]$  emission from the broad and narrow line regions, measurable with *JWST* in the future). The fact that we do not see enhanced FIR  $[\text{O III}]_{88}$  emission in J2100–Q indicates that its  $[\text{O III}]_{88}$  emission is dominated by star formation, and not AGN activity. This is supported by the finding that the linewidths and positions of the  $[\text{O III}]_{88}$  and  $[\text{C II}]$  line are the same in both sources and consistent with previous findings that the ISM properties in distant quasar host galaxies are predominantly powered by star formation (e.g., Leipski et al. 2014; Barnett et al. 2015; Venemans et al. 2017). One caveat is that J2100–SB could in principle also

host an *obscured* accreting supermassive black hole. In that case, the  $[\text{O III}]_{88}$  emission in the companion may not be solely due to star formation. However, the fact that the  $[\text{O III}]_{88}/\text{FIR}$  and  $[\text{O III}]_{88}/[\text{C II}]$  luminosity ratios of J2100–SB lie within the range of local LIRGs (including those that are not dominated by an AGN) argues against such a scenario. This latter finding, together with our analysis of the number of photons needed for the creation of  $\text{O}^{++}$ , implies that no extreme (top-heavy) initial stellar mass functions are needed to explain the  $[\text{O III}]_{88}$  luminosity in our sources.

We thank the referee for helpful comments that improved our manuscript and Gordon Stacey for useful suggestions. F.W., B.V., M.N., and Ma.N. acknowledge support from the ERC Advanced grant 740246 (Cosmic\_Gas). D.R. acknowledges support from the National Science Foundation under grant No. AST-1614213. R.W. acknowledges supports from the National Science Foundation of China (11721303). This Letter makes use of the following ALMA data: ADS/JAO.ALMA#2017.1.00118.S, ADS/JAO.ALMA#2015.1.01115.S. ALMA is a partnership of ESO (representing its member states), NSF (USA) and NINS (Japan), together with NRC (Canada), NSC and ASIAA (Taiwan), and KASI (Republic of Korea), in cooperation with the Republic of Chile. The Joint ALMA Observatory is operated by ESO, AUI/NRAO and NAOJ. The National Radio Astronomy Observatory is a facility of the National Science Foundation operated under cooperative agreement by Associated Universities, Inc.

*Facility:* ALMA.

*Software:* CASA (McMullin et al. 2007).

## ORCID iDs

Fabian Walter <https://orcid.org/0000-0003-4793-7880>  
 Dominik Riechers <https://orcid.org/0000-0001-9585-1462>  
 Roberto Decarli <https://orcid.org/0000-0002-2662-8803>  
 Carl Ferkinhoff <https://orcid.org/0000-0001-6266-0213>  
 Bram Venemans <https://orcid.org/0000-0001-9024-8322>  
 Frank Bertoldi <https://orcid.org/0000-0002-1707-1775>  
 Xiaohui Fan <https://orcid.org/0000-0003-3310-0131>  
 Emanuele Farina <https://orcid.org/0000-0002-6822-2254>  
 Chiara Mazzucchelli <https://orcid.org/0000-0002-5941-5214>

Marcel Neeleman  <https://orcid.org/0000-0002-9838-8191>  
 Michael A. Strauss  <https://orcid.org/0000-0002-0106-7755>  
 Bade Uzgil  <https://orcid.org/0000-0001-8526-3464>  
 Ran Wang  <https://orcid.org/0000-0003-4956-5742>

## References

- Baldwin, J. A., Phillips, M. M., & Terlevich, R. 1981, *PASP*, 93, 5  
 Bañados, E., Venemans, B. P., Decarli, R., et al. 2016, *ApJS*, 227, 11  
 Barnett, R., Warren, S. J., Banerji, M., et al. 2015, *A&A*, 575, A31  
 Bertoldi, F., Cox, P., Neri, R., et al. 2003, *A&A*, 409, L47  
 Brauher, J. R., Dale, D. A., & Helou, G. 2008, *ApJS*, 178, 280  
 Carilli, C. L., & Walter, F. 2013, *ARA&A*, 51, 105  
 Carniani, S., Maiolino, R., Pallottini, A., et al. 2017, *A&A*, 605, A42  
 Chabrier, G. 2003, *PASP*, 115, 763  
 da Cunha, E., Groves, B., Walter, F., et al. 2013, *ApJ*, 766, 13  
 Decarli, R., Walter, F., Venemans, B. P., et al. 2017, *Natur*, 545, 457  
 Decarli, R., Walter, F., Venemans, B. P., et al. 2018, *ApJ*, 854, 97  
 De Looze, I., Cormier, D., Lebouteiller, V., et al. 2014, *A&A*, 568, A62  
 Díaz-Santos, T., Armus, L., Charmandaris, V., et al. 2017, *ApJ*, 846, 32  
 Draine, B. T., Dale, D. A., Bendo, G., et al. 2007, *ApJ*, 663, 866  
 Fan, X., Strauss, M. A., Becker, R. H., et al. 2006, *AJ*, 132, 117  
 Ferkinhoff, C., Hailey-Dunsheath, S., Nikola, T., et al. 2010, *ApJL*, 714, L147  
 Ferkinhoff, C., Brisbin, D., Nikola, T., et al. 2011, *ApJL*, 740, L29  
 Ferkinhoff, C., Brisbin, D., Nikola, T., et al. 2015, *ApJ*, 806, 260  
 Hashimoto, T., Inoue, A. K., Mawatari, K., et al. 2018a, arXiv:1806.00486  
 Hashimoto, T., Laporte, N., Mawatari, K., et al. 2018b, *Natur*, 557, 392  
 Inoue, A. K., Tamura, Y., Matsuo, H., et al. 2016, *Sci*, 352, 1559  
 Kennicutt, R. C., & Evans, N. J. 2012, *ARA&A*, 50, 531  
 Kramida, A., Ralchenko, Y., Nave, G., & Reader, J. 2018, APS Division of Atomic, Molecular and Optical Physics Meeting Abstracts, 2018, M01.004  
 Kroupa, P. 2001, *MNRAS*, 322, 231  
 Laporte, N., Nakajima, K., Ellis, R. S., et al. 2017, *ApJ*, 851, 40  
 Leipski, C., Meisenheimer, K., Walter, F., et al. 2014, *ApJ*, 785, 154  
 Marrone, D. P., Spilker, J. S., Hayward, C. C., et al. 2018, *Natur*, 553, 51  
 McMullin, J. P., Waters, B., Schiebel, D., Young, W., & Golap, K. 2007, in ASP Conf. Ser. 376, *Astronomical Data Analysis Software and Systems XVI*, ed. R. A. Shaw, F. Hill, & D. J. Bell (San Francisco, CA: ASP) 127  
 Sandstrom, K. M., Leroy, A. K., Walter, F., et al. 2013, *ApJ*, 777, 5  
 Savage, B. D., & Sembach, K. R. 1996, *ApJ*, 470, 893  
 Tamura, Y., Mawatari, K., Hashimoto, T., et al. 2018, arXiv:1806.04132  
 Vacca, W. D., Garmany, C. D., & Shull, J. M. 1996, *ApJ*, 460, 914  
 Vanden Berk, D. E., Richards, G. T., Bauer, A., et al. 2001, *AJ*, 122, 549  
 Venemans, B. P., Verdoes Kleijn, G. A., Mwebaze, J., et al. 2015, *MNRAS*, 453, 2259  
 Venemans, B. P., Walter, F., Decarli, R., et al. 2017, *ApJ*, 845, 154  
 Venemans, B. P., Decarli, R., Walter, F., et al. 2018, *ApJ*, 866, 159  
 Vishwas, A., Ferkinhoff, C., Nikola, T., et al. 2018, *ApJ*, 856, 174  
 Walter, F., Bertoldi, F., Carilli, C., et al. 2003, *Natur*, 424, 406  
 Walter, F., Riechers, D., Cox, P., et al. 2009, *Natur*, 457, 699  
 Wang, R., Wagg, J., Carilli, C. L., et al. 2013, *ApJ*, 773, 44  
 Willott, C. J., Albert, L., Arzoumanian, D., et al. 2010a, *AJ*, 140, 546  
 Willott, C. J., Delorme, P., Reylé, C., et al. 2010b, *AJ*, 139, 906  
 Willott, C. J., Omont, A., & Bergeron, J. 2013, *ApJ*, 770, 13  
 Willott, C. J., Bergeron, J., & Omont, A. 2015, *ApJ*, 801, 123  
 Wu, X.-B., Wang, F., Fan, X., et al. 2015, *Natur*, 518, 512